POWER-INSENSITIVE SILICON CRYSTAL-CUT FOR AMPLITUDE-STABLE FREQUENCY SYNTHESIS

Mayur Ghatge, Pratyusha Karri, and Roozbeh Tabrizian
Interdisciplinary Microsystems Group, University of Florida
Gainesville, FL, USA

ABSTRACT

This paper reports on the theoretical prediction and experimental verification of the existence of a power-insensitive crystal cut in doped single crystal silicon (SCS). The existence of such a cut enables fully harmonic excitation of extensional elastic waves with negligible dispersion. Aligning bulk acoustic resonators to this power-insensitive cut along with suppression of boundary-induced nonlinearities enable realization of vibration-amplitude insensitive frequency references. An analytical formulation is presented to characterize the anisotropic anharmonic behavior of SCS elasticity, predicting the existence of the power-insensitive cut at ~30° offset from <100> axis. This prediction is experimentally verified through implementation and characterization of an array of waveguide-based resonators aligned to different crystallographic directions. The resonators are optimized for substantial suppression of boundary induced nonlinearities through dispersive energy trapping technique. Among these, the waveguide-based resonator aligned to 22.5° cut shows a 1-dB compression point at 29dBm, which is 50× higher power-handling compared to <100> / <110> counterparts. Dispersive energy trapping used for elimination of geometrical nonlinearities simultaneously realizes a high *Q* of ~7,000 at 80MHz, which is independent of the crystallographic orientation.

INTRODUCTION

The application of MEMS resonators for RF reference generation and signal processing has been limited by the inevitably poor power handling capability of the devices imposed by their miniaturized form factor [1-3]. The power handling capability of a MEMS resonator is defined by the upper limit of its linear operation dynamic range. The nonlinear distortion of MEMS resonator operation is a combinatorial result of anharmonicities in electromechanical transduction, energy dissipation and material elastic characteristics. Among these, elastic anharmonicity is an inherent characteristic of materials and is a result of highly nonlinear inter-atomic / -molecular forces.

The efforts on linear dynamic range extension of MEMS resonators have focused on replacing nonlinear transducers with linear counterparts [4-6], increasing resonators' mechanically active volume [7], addition of supporting tethers for suppression of geometrical nonlinearities [8], and application of single crystals with larger linear elastic operation range [3][9]. Although successful with incremental improvements in power handling capability, these methods are eventually bounded by the intrinsic elastic anharmonicity of thin films and single crystals.

In this work, we report on the existence of a fully-harmonic crystal cut in doped single crystal silicon that can essentially remove the intrinsic upper bound of the power handling in MEMS resonators and extend it all the way to the elastic / plastic yield point of the crystal. We further utilize this cut, along with dispersive energy trapping techniques for elimination of boundary induced nonlinearities, to realize high *Q* resonators for amplitude-stable frequency references.

ELASTIC ANHARMONICTY

The inter-atomic binding forces in solids are highly non-linear and thus the elastic properties in solids are anharmonic; i.e. elastic excitations at a frequency ω induces deformations with higher order harmonics (2ω, 3ω, etc.) along with the fundamental frequency (ω). In anisotropic semiconductors, such elastic anharmonicity is anisotropic and depends significantly on the doping type and concentration [2][10].

In the simplest form, the nonlinear elastic behavior can be shown in a rod with an infinitesimally small cross-section through engineering elastic moduli:

$$\sigma = \lambda_0\epsilon + \lambda_1\epsilon^2 + \lambda_2\epsilon^3 \quad (1)$$

where σ and ϵ are induced stress and strain, and λ_0 and $\lambda_{1,2}$ are linear and nonlinear engineering moduli respectively. When exciting a mechanical vibration in the rod with a sufficiently large amplitude, (1) not only results in the excitation of higher frequency harmonics, but also induces a shift in the resonance frequency (f_0) that is proportional to the vibration amplitude (X_0) square [11]:

$$f_{0,non-linear} = f_{0,linear}(1 + \kappa X_0^2) \quad (2)$$

where κ, the amplitude-frequency (A-f) coefficient, can be related to linear / nonlinear engineering moduli in a pure extensional / shear vibration mode through [10]:

$$\kappa = \frac{9\pi^2\lambda_2}{32\lambda_0 L^2} - \frac{80\lambda_1^2}{27L^2\lambda_0^2} \quad (3)$$

where *L* is the length of the rod. While (2) and (3) suggest the application of resonators for extraction of anharmonic elastic constants, in practice the accuracy of such a technique depends on sufficient suppression of geometrical and boundary induced nonlinearities. Furthermore, as illustrated in (3), extraction of κ can only provide a nonlinear relation between λ_i $(i = 0,1,2)$, rather than facilitating their independent extraction. To further extract individual λ_i values, (3) can be extended to a system of equations that relate linear and nonlinear elastic moduli with frequency variations of resonant rods aligned to different crystallographic directions. Such a system along with crystal co-ordinates transformation can be used to extract λ_i values for different crystal cuts. The corresponding equations for extraction of nonlinear Young's moduli is shown in (4).

$$\kappa_\theta = \frac{9\pi^2 E_{2,\theta}}{32 E_{0,\theta} L^2} - \frac{80 E_{1,\theta}^2}{27 L^2 E_{0,\theta}^2};\ \widehat{E_\theta}(\epsilon) = E_{0,\theta} + E_{1,\theta}\epsilon + E_{2,\theta}\epsilon^2$$

$$\frac{1}{\widehat{E_\theta}(\epsilon)} = \frac{c^4}{\widehat{E_0}(c^2\epsilon)} + \frac{s^4}{\widehat{E_0}(s^2\epsilon)} - \frac{s^2c^2}{2G_{0,\pi/4}}\left\{\frac{\widehat{E_0}(c^2\epsilon) - 2G_{0,\pi/4}}{\widehat{E_0}(s^2\epsilon)} - \frac{\widehat{E_0}(s^2\epsilon) - 2G_{0,\pi/4}}{\widehat{E_0}(c^2\epsilon)}\right\} + \frac{s^2c^2}{\widehat{G_0}(sc\epsilon)} \qquad (4).$$

Here, $\widehat{E_\theta}(\epsilon)$ and $\widehat{G_\theta}(\epsilon)$ are the nonlinear Young's and shear moduli for θ-cut, in <100> plane and with respect to <010> crystal axis with $E_{i,\theta}$ and $G_{i,\theta}$ $(i = 0,1,2)$ the linear / nonlinear coefficients; c and s are directional cosines and sines of θ-cut (i.e. $c = \cos(\theta)$ and $s = \sin(\theta)$). (4) can be used, along with basic resonant test-structures aligned to <100> and <110>, to extract $E_{i,\theta}$ for different crystal cuts. These values are summarized for $\theta = 0$ and 45° (i.e. <100> and <110> crystal cuts) in Table 1.

Table 1: Nonlinear Young's moduli in major axes of Si.

	<100>	**<110>**
$\|E_1/E_0\|$	85.4	54.5
$\|E_2/E_0\|$	7916	3131

The results for $E_{i,\theta}$ can be used to extract κ_θ. Figure 1 shows κ_θ normalized with respect to $\left(\frac{X_0}{L}\right)^2$ to demonstrated the relative A-f coefficient in arbitrary θ-cut of the (100) plate of N-doped SCS. As inferred from Figure 1, while <100> and <110> major crystal directions show highly positive and negative A-f coefficient, at $\theta \approx 30°$, κ vanishes indicating the fully-harmonic characteristic of the extensional waves aligned to this cut.

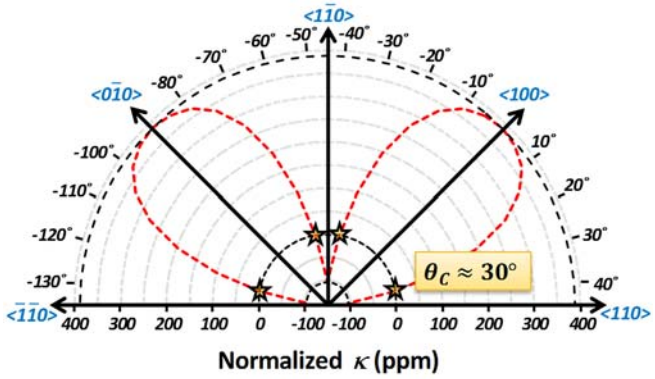

Figure 1: Analytically extracted normalized amplitude-frequency coefficient (κ) in different crystal cuts of (100) N-doped Si, suggesting the power-insensitive cut at $\theta_C \approx 30°$.

DISPERSIVE ENERGY TRAPPING

The application of the fully-harmonic crystal cut for realization of power-insensitive resonators depends on suppression of extrinsic nonlinearity effects induced by resonator boundaries (i.e. geometrical effects). While these effects can be negligible in devices aligned to major symmetric crystal axes of silicon (i.e. <100> and <110>) [2], they cannot be neglected, and can even be significant, when aligned to non-symmetric crystal cuts. Figure 2 compares the mode shape of silicon bulk acoustic resonators (SiBAR) aligned to 0° and 45° (i.e. <110> and <100>) and 22.5°, suggesting considerable non-axisymmetric distortion in extensional mode shape for the 22.5° oriented device. Such a distortion is a result of nonzero c_{16} component of the rotated crystal elastic matrix, which internally couples symmetric extensional excitations to non-symmetric shear deformations that do not have a nodal point at the supporting tethers. This incompatibility of the mixed shear-extensional mode with anchoring points not only degrades the Q significantly, but also amplifies the energy concentration at narrow-tether area. Such an increased energy concentration makes the device highly prone to boundary induced nonlinearities that initiates from nonlinear deformation of narrow tethers [12][13].

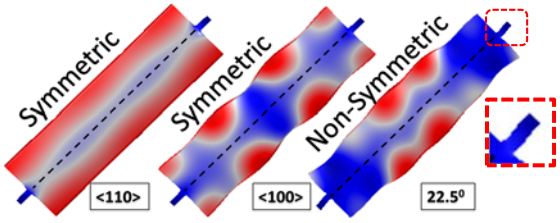

Figure. 2: Mode shapes of SiBARs aligned to 0°, 45°, *&* 22.5°, *highlighting the non-symmetric distortion as well as amplified energy concentration in tether regions for* 22.5° *aligned device.*

To obviate narrow tethers, dispersive energy trapping can be used to realize high Q resonators that are essentially insensitive to boundary induced nonlinearities. In this approach [14], dispersive characteristic of Lamb waves is used in geometrically-engineered waveguides to couple propagating and evanescent waves. This results in efficient energy trapping in the central region of the device and far from flanks. Dispersive energy trapping technique can be similarly applied to waveguides aligned to arbitrary crystal directions through utilization of corresponding dispersion curves. Figure 3 compares the dispersion curves of 1st width-extensional and 2nd width-shear branches for various crystal cuts (<100>, <110>, and 22.5°), demonstrating their similar dispersive characteristics. Figure 3 also highlights the effect of width variation on the transformation of the dispersion curves for 22.5° cut. Such a width-dependency is used to couple propagating waves in the central region to evanescent waves, with exponentially decaying energy, in the flanks. Such a waveguide-based resonator design eliminates the need for a nodal point and thus the requirement of narrow tether supports. This in-turn eliminates distortions at the supports

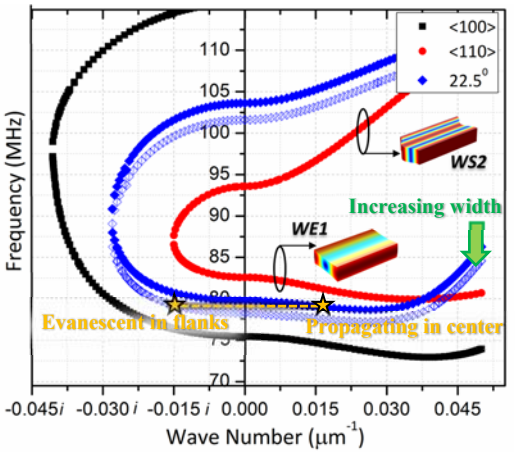

Figure 3: Dispersion Characteristics of Si waveguide oriented along <100>, <110> and 22.5°crystal cuts. The shaded blue branch belongs to the wider waveguide of the device oriented at 22.5° (evanescent region).

and corresponding boundary-induced nonlinear effects. Figure 4 demonstrates the mode shape as well as acoustic energy distribution in a waveguide-based resonator aligned to the 22.5° cut, highlighting the efficient energy trapping.

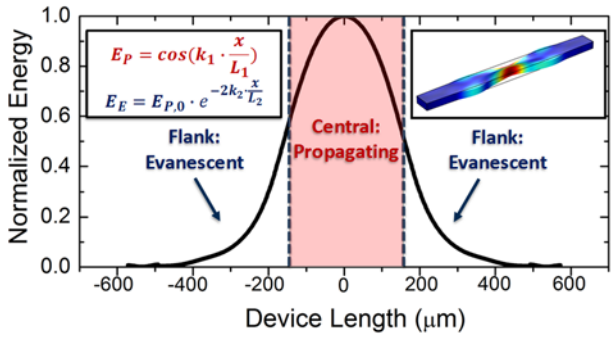

Figure 4: Simulated elastic energy density along the central axis of the device. Inset shows COMSOL simulated vibration mode and energy density functions in central (propagating) and flank (evanescent) regions.

RESONATOR ARRAY IMPLEMENTATION

To experimentally study the anisotropic elastic anharmonicity, an array of waveguide-based resonators that are oriented to different crystal cuts is implemented. Each of the resonators are designed individually using corresponding dispersion curves to guarantee suppression of boundary induced nonlinearities, as well as orientation-independent high Q's. Devices are implemented in 0.0015 Ω.cm phosphorous-doped Si substrate with a thickness of 30μm, and integrated with 500nm AlN film, and through a similar process flow used in [14]. The piezoelectric transduction scheme is used to benefit from its superior linear characteristic compared to capacitive counterparts. Figure 5 shows the SEM image of the resonator array as well as the 22.5° oriented device. This device, along with <100> and <110> counterparts are used to experimentally verify the theoretical prediction of the existence of fully-harmonic crystal cut in doped single crystal silicon.

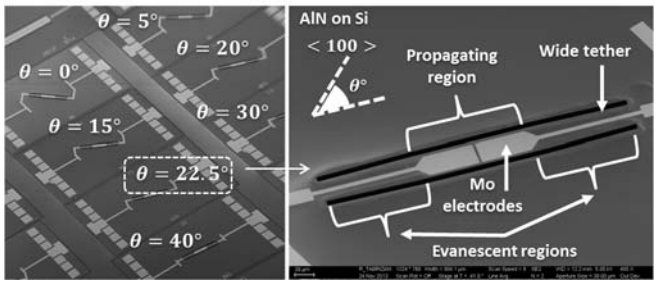

Figure 5: SEM images of (left) array of waveguide-based resonators aligned to different crystal cuts in (100) Si; (right) the 22.5° device designed using dispersive energy trapping.

CHARACTERIZATION & VERIFICATION

Implemented waveguide-based resonators are characterized to verify their efficiency of energy trapping, and analyzed for their power handling capability with IP3 and 1-dB compression-point measurements. Figure 6 shows the measured frequency response of the 22.5°-oriented device. A Q of ~7,000 is measured at f_0 of 80 MHz with an insertion loss of ~23 dB, confirming the efficiency of energy trapping. To the knowledge of authors, this is the first demonstration of a high-Q BAW Si resonator that is not aligned to the major crystal axes. A consistent Q with a slight ±10% variation is measured for the entire array verifying the orientation-independence of dispersive energy trapping technique.

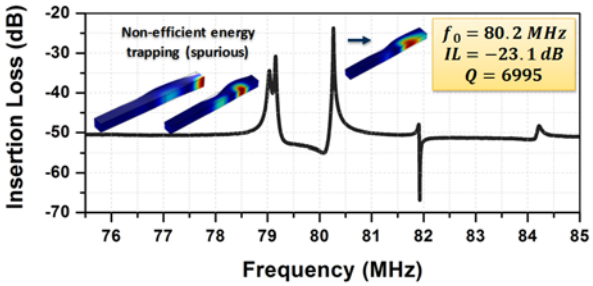

Figure 6: Measured frequency response for θ = 22.5°, with a ~8 dB higher insertion loss in lower frequency spurs.

Figure 7 compares the frequency shift as a function of input power between θ = 0°, 45° and 22.5° resonators, showing a significantly lower sensitivity of f_0 to vibration amplitude for θ = 22.5°, compared to all other counterparts in the array. This closely confirms the analytically predicted fully-harmonic crystal cut at $\theta_C \approx 30°$. The slight discrepancy can be attributed to the effect of AlN film and alignment imperfections / residual geometrical nonlinearities.

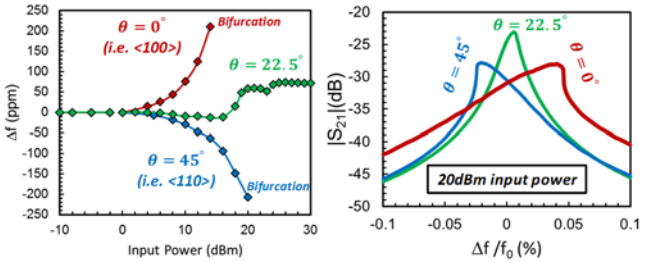

Figure 7: (left) Anharmonicity-induced f_0 shift vs. input power and (right) frequency response distortion with 20dBm input power for resonators aligned to θ = 0°, 45° and 22.5°.

Figure 8(a-c), shows the three-tone power measurements for resonators oriented along <100>, <110> and 22.5°. The large 2nd and 3rd intermodulation intercept points of ~90dBm and ~80dBm are measured for the three devices is a result of thick (30µm) silicon substrate. The 1-dB compression point for the device oriented to 22.5° is 29 dBm, while that of the <110> and <100> oriented devices are 19 dBm and 15 dBm, respectively. This ~50-fold improvement in the power handling is attributed to the harmonic nature of the 22.5° crystal cut in doped Si. Finally, Figure 8(d) compares the measured power compression between <100> and 22.5°, showing two extremes of elastic anharmonicity and confirming analytical predictions (Figure 1).

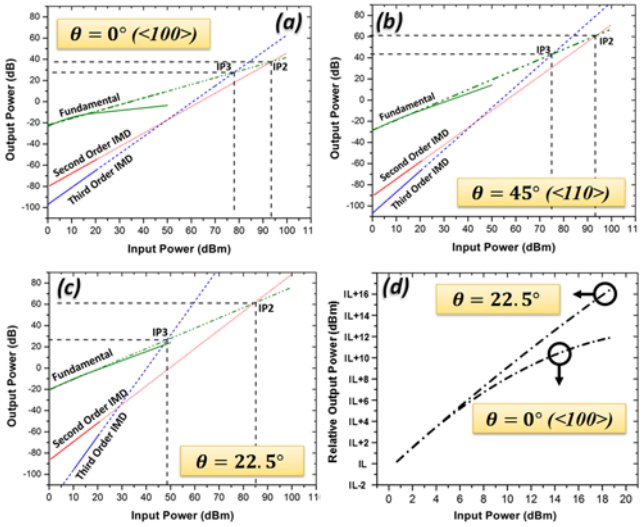

Figure 8: Three-tone power measurement for resonators aligned to (a) θ = 0°, (b) θ = 45° and (c) θ = 22.5° cuts in (100) Si plane. (d) Comparison of measured compression for extreme cases of <100> (highly anharmonic) and 22.5° (highly harmonic) relative to the output power.

CONCLUSION

This paper presents the theoretical prediction and experimental demonstration of the existence of a power-insensitive crystal-cut in N-doped silicon. For the first time a formulation for analytical characterization of the anisotropic elastic anharmonicity is presented, predicting the existence of a fully-harmonic crystal-cut at ~30° offset from the <100> axis in (100) plane. An array of high *Q* resonators aligned to various crystal cuts are implemented for experimental verification. Dispersive energy trapping is used for realization of test-vehicles to substantially suppress geometrical nonlinearities and enable accurate monitoring of the elastic anharmonicities. Among these, the resonator aligned to 22.5° cut demonstrated a superior power-handling capability with 50× improvement compared to <100> / <110> counterparts, thus validating the theoretical predictions of the existence of a power-insensitive crystal cut.

ACKNOWLEDGEMENTS

The authors thank the staff at Nanoscale Research Facility at the University of Florida for their help with the device fabrication.

REFERENCES

[1] Hashimoto, & Ken-ya. *RF bulk acoustic wave filters for communications*. Artech House, 2009.

[2] Kaajakari, Ville, et al. "Nonlinear mechanical effects in silicon longitudinal mode beam resonators." *Sensors and Actuators A: Physical* 120.1 (2005): 64-70.

[3] Gokhale, V. J., J. Roberts, & M. Rais-Zadeh. "High performance bulk mode gallium nitride resonators and filters." *2011 16th International Solid-State Sensors, Actuators and Microsystems Conference*. IEEE, 2011.

[4] Zuo, C., Rinaldi, M., & Piazza, G. "Power handling and related frequency scaling advantages in piezoelectric AlN contour-mode MEMS resonators". (2009): 1187

[5] Agarwal, M., Park, K., Candler, R., Hopcroft, M., Jha, C., Melamud, R., et al. (2005, December). "Non-linearity cancellation in MEMS resonators for improved power handling". In *Proceedings of the IEDM* (pp. 286-289).

[6] Thakar, Vikram A., et al. "Piezoelectrically transduced temperature-compensated flexural-mode silicon resonators." *JMEMS* 22.3 (2013): 815 -823.

[7] Abdolvand, R., & Ayazi, F. (2007, October). "7E-4 enhanced power handling and quality factor in thin-film piezoelectric-on-substrate resonators". In *Ultrasonics Symposium, 2007. IEEE* (pp. 608-611). IEEE.

[8] Shahmohammadi, M., Harrington, B. P., & Abdolvand, R. (2010, May). "Concurrent enhancement of Q and power handling in multi-tether high-order extensional resonators". In *Microwave Symposium Digest (MTT), 2010 IEEE MTT-S International* (pp. 1452-1455). IEEE.

[9] Fatemi, H., & Abdolvand, R. "Fracture limit in thin-film piezoelectric-on-substrate resonators: Silicon VS. diamond". In *Micro Electro Mechanical Systems (MEMS), 2013 IEEE 26th International Conference on* (pp. 461-464). IEEE.

[10] Yang, Yushi, et al. "Measurement of the nonlinear elasticity of doped bulk-mode MEMS resonators." *Solid-state sensors, actuators and* microsystems *workshop, Hilton Head Island, South Carolina*. 2014.

[11] Landau, L. D., & E. M. Lifshitz. "Resonance in non-linear oscillations." *Mechanics* 1: 87-92.

[12] Lifshitz, R., & Cross, M. C. *Reviews of nonlinear dynamics and complexity.* H. G. Schuster (Ed.). Wiley-VCH-Verlag.

[13] Davis, W. O., O'Reilly, O. M., & Pisano, A. P. (2004). On the nonlinear dynamics of tether suspensions for MEMS. *Journal of vibration and acoustics*, *126*(3), 326-331.W. P. Eaton, et. al., "Micromachined pressure sensors: review and recent developments", Smart Materials and Structures 6.5 (1997), pp. 530-539.

[14] Ghatge, M., & Tabrizian, R., "Bilayer Nano-Waveguide Resonators for Sensing Applications," *Proc. 2016 IEEE Sensors Conference,* Nov. 2016, pp. 1601-1603

CONTACT

*M Ghatge, tel: +1-614-377-7228; ruyam@ufl.edu